

Article

An Analytical Solution for the Geometry of High-Speed Railway CRTS III Slab Ballastless Track

Lili Liu ¹, Lizhong Jiang ^{1,2}, Wangbao Zhou ^{1,2,*} , Xiang Liu ³ and Yulin Feng ⁴¹ School of Civil Engineering, Central South University, Changsha 410075, China² National Engineering Research Center of High-Speed Railway Construction Technology, Changsha 410075, China³ School of Civil Engineering, Fujian University of Technology, Fuzhou 350118, China⁴ School of Civil Engineering and Architecture, East China Jiaotong University, Nanchang 330013, China

* Correspondence: zhouwangbao@163.com

Abstract: To study the mapping relationship between girder deformation and rail deformation for the CRTS III slab ballastless track (SBT) multi-span simply supported bridge, this study derived a simplified analytical solution, and the corresponding ANSYS finite element model (AFEM) was established. Compared with the fine analytical model (FAM) and the AFEM, the calculation results of the three models under the conditions of pier settlement and girder vertical fault were compared, which verified the universal properties of the simplified analytical model (SAM). Based on the verified SAM, the influence of pier settlement, fastener stiffness, girder span, and girder vertical fault on rail deformation was studied. The results show that the rail deformation is approximately proportional to pier settlement and girder vertical fault. With the increase in fastener stiffness, the fastener internal force increases, the rail mapping deformation increases, and the length of the rail mapping deformation area decreases. With the increase in girder span, the rail deformation curve becomes smooth, the length of the rail mapping deformation area becomes longer, and the fastener internal force is significantly reduced.



Citation: Liu, L.; Jiang, L.; Zhou, W.; Liu, X.; Feng, Y. An Analytical Solution for the Geometry of High-Speed Railway CRTS III Slab Ballastless Track. *Mathematics* **2022**, *10*, 3306. <https://doi.org/10.3390/math10183306>

Academic Editor: Fernando Simoes

Received: 4 August 2022

Accepted: 8 September 2022

Published: 12 September 2022

Publisher's Note: MDPI stays neutral with regard to jurisdictional claims in published maps and institutional affiliations.



Copyright: © 2022 by the authors. Licensee MDPI, Basel, Switzerland. This article is an open access article distributed under the terms and conditions of the Creative Commons Attribution (CC BY) license (<https://creativecommons.org/licenses/by/4.0/>).

Keywords: CRTS III SBT system; mapping deformation; principle of stationary potential energy; analytical model; numerical simulation

MSC: 37N15

1. Introduction

Ballastless track structure is commonly used in China's high-speed railways to meet the requirements of high levelness and stability [1]. In the past few years, the structural forms of ballastless track structures include CRTS I SBT, CRTS II SBT, and CRTS III SBT [2]. CRTS III SBT inherits the advantage of CRTS I SBT and CRTS II SBT, which is the optimization and integration of the existing ballastless track [2]. Nowadays, CRTS III SBT is widely used in high-speed railway systems. Due to the special geological conditions and environmental factors in China, "replacing roads with bridge" is widely adopted [3]. Therefore, the length of high-speed railways in special areas, such as active seismic zones, foundation settlements, and extreme climates are getting longer and longer [4,5]. The bridge structure will inevitably suffer from pier tilt, girder vertical fault, girder corner, and bearing damage [6,7]. When the bridge deformation occurs, the various layers of the ballastless track will undergo a certain follow-up settlement under the action of gravity, which will cause the rail deformation [8]. In severe cases, it may cause the train to derail, affecting the riding comfort and driving safety [9–11].

It is obvious that one of the key factors affecting the change in rail surface geometry is girder deformation. The important prerequisite of studying the influence of girder deformation on the safety and stability of high-speed trains is exploring the mapping

relationship between the girder and rail. Varandas et al. [12], Galvín et al. [13] and Ju et al. [14] established a novel computer implementation that can consider nonlinear contact relations between CRTS SBT components, focusing on the estimation of ballast and sub-ballast long-term deformations. The actual behavior of the structure can be easily and accurately reproduced. Feng et al. [15] describes a study of the mapping relationship between the girder vertical deformation and rail deformation. The results show that the mapping coefficient between girder vertical deformation and rail deformation showed a nonlinear increase with the increasing of girder vertical deformation. The shape of the rail deformation curve has obvious “followability”; with the increase in fastener stiffness and girder span, the rail mapping deformation curve tends to flatten out, and the length of the mapping deformation area of the rail increases. Gou et al. [16] established an analysis model of the mapping relationship between bridge deformation and rail deformation based on the balance of classical mechanics, and verified it with finite elements. The key parameters affecting the rail geometry are analyzed. The results show that the analytical method of rail mapping deformation derived from the theory can predict the rail geometry accurately. Rail mapping deformation increases with the increase in pier settlement and girder vertical fault. The greater the stiffness of the fasteners or mortar layer is, the greater the mapping deformation of the rails is and the smaller the smoothness of the track is, the greater the danger to the running safety and ride comfort of the high-speed railway is. Al Shaer et al. [17] designed an experiment in order to investigate the dynamic behavior and the settlement of ballasted tracks. The results show that the stiffness of the track changes during the experiment. Settlement deformation is a function related to acceleration. Lai et al. [18] presented an analytical method to describe the geometry status of the track. The contribution of system parameters to rail geometry was investigated. The results show that the effect of shear grooves on the mapped deformation of rails is significant. The stiffness of the cemented asphalt layer and sliding layer contribute significantly to the rail mapping deformation. Ahmari et al. [19] adopted the Hamilton principle to derive the vibration control equations for a linearly supported orthotropic anisotropic thin plate under the action of moving vehicles. The effect of the foundation settlement on the train–bridge dynamic interaction was investigated by correcting for the forces caused by bridge deck deformation. The results show that the influence of bearing settlement deformation on the train–bridge dynamic interaction is significant. Chen et al. [20] derived the mapping relationship between rail deformation and pier settlement theoretically, and verified it by finite element analysis. The rail unevenness caused by bridge pier settlement is superimposed on the track’s random initial unevenness, and the superimposed rail unevenness is input to the train–track–bridge model as an excitation, and the influence law of bridge pier settlement amplitude on vehicle dynamic indexes is analyzed. Based on the limits of running safety and the ride comfort indexes of high-speed trains, the proposed threshold value of bridge pier settlement deformation is proposed.

In summary, the mapping relationship between bridge structure deformation and track surface deformation is very significant for the study of driving safety [21–23]. At present, there is little research on the mapping relationship between bridge structure deformation and the rail surface deformation of the CRTS III SBT system at home and abroad. In order to study the mapping relationship between bridge structure deformation and rail deformation, this paper uses the CRTS III SBT multi-span simply supported bridge as the research object, based on the principle of stationary potential energy, and deduces an analytical model of the mapping relationship between bridge structure deformation and rail deformation [1]. Further, the corresponding ANSYS finite element model is established for verification. In addition, a parametric analysis of the influencing factors affecting rail unevenness is carried out.

2. The Mapping Relationship between Girder Deformation and Rail Deformation

2.1. Mechanism Analysis of Rail Deformation Caused by Girder Deformation

This study takes the CRTS III SBT simply supported bridge system as the research object. The CRTS III SBT simply supported bridge system is shown in Figure 1. The CRTS III SBT is composed of three layers of concrete slabs, namely: the bidirectional prestressed concrete track slab (concrete strength grade is C60); self-compacting concrete filling layer (SCCFL) (concrete strength grade is C40); and the concrete base slab (concrete strength grade is C40). An isolation layer is formed between the composite slab and the base slab by laying a 4 mm thick geotextile. The track system connects the girder with the concrete base slab through pre-embedded steel bars. Each base slab is provided with two grooves, with a rectangle section of 1000×700 mm and a groove depth of 100 mm. The SCCFL is poured on site. During the pouring process, two limit convex platforms are formed at the lower part of the SCCFL corresponding to the groove of the base slab. The inside of the groove is closely attached to the 8 mm rubber pad, and the 4 mm-thick geotextile is laid between the base slab and the SCCFL. U-shaped connecting steel is set to strengthen the connection between the SCCFL and the track slab. According to the structural characteristics of the CRTS III SBT system, it is known that when the simply supported bridge is vertically deformed due to the external environment, such as foundation settlement, earthquake, and so on, the CRTS III SBT system, which is laid on the deformed girder, will produce following deformation under the action of interlayer force and gravity.

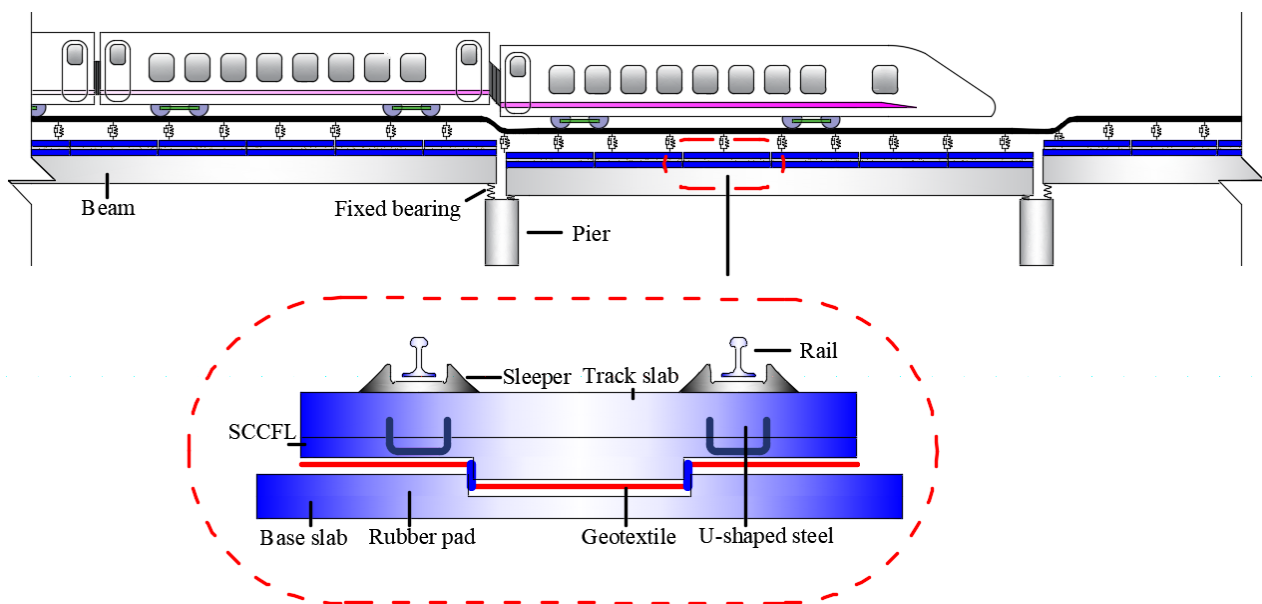


Figure 1. Schematic diagram of the CRTS III SBT structure.

2.2. Basic Assumptions

In order to establish the mapping relationship model between girder deformation and rail deformation of the CRTS III SBT system, the following assumptions are made:

- (1) The gravitational equilibrium state of the system is taken as the initial state and the gravity effect is neglected during the calculation.
- (2) The base slab and the girder are connected by pre-embedded steel bars, which have a strong inter-layer restraint effect, and the CRTS III SBT system forms a composite plate due to its own strong inter-layer connection. Therefore, it is assumed that the CRTS III SBT system is coordinated with the deformation of the girder.
- (3) This paper ignores the influence of CRTS III SBT structure on the girder deformation, because the vertical bending stiffness of the girder is extremely large.

- (4) The rails in the subgrade are reduced to simply supported boundaries, and the boundary effect of the rail is eliminated by taking enough effective length of the subgrade.
- (5) The fastener is considered as a linear spring uniformly distributed along the centerline of the rail.

2.3. The Basic Equation of Mapping

Assuming that the number of CRTS III SBT is M , each span and subgrade are arranged with six CRTS III SBT, and each CRTS III SBT has N fasteners, then there are MN fasteners and $\frac{M}{6} - 2$ simply supported girders.

2.3.1. Rail Displacement

According to the above assumptions, it can be known that the mechanical model of the rail is shown in the Figure 2.

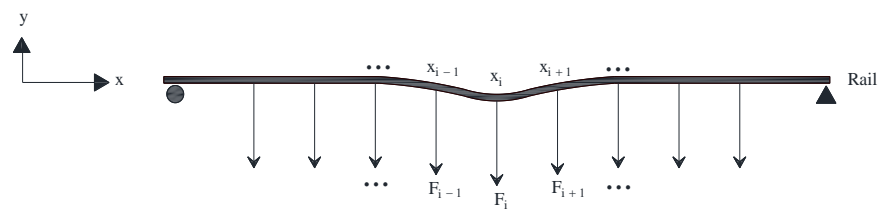


Figure 2. Mechanical model of rail.

Assuming that when the pier settles, the vertical deformation of the rail with the pier settlement is ω_1 . So, the simply supported boundary condition of the rail can be expressed as:

$$\begin{cases} \omega_1(x=0) = 0 \\ \omega_1(x=l_g) = 0 \\ \omega_1''(x=0) = 0 \\ \omega_1''(x=l_g) = 0 \end{cases} \tag{1}$$

where l_g is the total length of the rail.

Further, taking the sine function as the basis function, the deformation curve of the rail with the pier settlement can be approximately expressed as follows:

$$\omega_1(x) = \sum_{m=1}^n A_m \sin\left(\frac{m\pi x}{l_g}\right) \tag{2}$$

where $A_m (m = 1, \dots, n)$ is any constant.

Further, the total potential energy of the rail under a fastener force can be expressed as follows:

$$\Pi = \frac{E_g I_g}{2} \int_0^{l_g} \left(\frac{d^2 \omega_1(x)}{dx^2}\right)^2 dx - \sum_{i=1}^{MN} \frac{1}{2} F_i \omega_1(x_i) \tag{3}$$

In addition:

$$\begin{aligned}
 & \int_0^{l_g} \left(\frac{d^2\omega_1(x)}{dx^2} \right)^2 dx \\
 &= \int_0^{l_g} \left[-A_1 \left(\frac{\pi}{l_g} \right)^2 \sin \left(\frac{\pi x}{l_g} \right) \right]^2 dx + \int_0^{l_g} \left[-A_2 \left(\frac{2\pi}{l_g} \right)^2 \sin \left(\frac{2\pi x}{l_g} \right) \right]^2 dx + \dots + \int_0^{l_g} \left[-A_n \left(\frac{n\pi}{l_g} \right)^2 \sin \left(\frac{n\pi x}{l_g} \right) \right]^2 dx \\
 &+ \int_0^{l_g} 2 \left[-A_1 \left(\frac{\pi}{l_g} \right)^2 \sin \left(\frac{\pi x}{l_g} \right) \right] \left[-A_2 \left(\frac{2\pi}{l_g} \right)^2 \sin \left(\frac{2\pi x}{l_g} \right) \right] dx \\
 &+ \int_0^{l_g} 2 \left[-A_1 \left(\frac{\pi}{l_g} \right)^2 \sin \left(\frac{\pi x}{l_g} \right) \right] \left[-A_3 \left(\frac{3\pi}{l_g} \right)^2 \sin \left(\frac{3\pi x}{l_g} \right) \right] dx + \dots \\
 &= \frac{A_1^2 \pi^4}{l_g^4} \int_0^{l_g} \sin^2 \left(\frac{\pi x}{l_g} \right) dx + \frac{A_2^2 2^4 \pi^4}{l_g^4} \int_0^{l_g} \sin^2 \left(\frac{2\pi x}{l_g} \right) dx + \dots + \frac{A_n^2 n^4 \pi^4}{l_g^4} \int_0^{l_g} \sin^2 \left(\frac{n\pi x}{l_g} \right) dx \tag{4} \\
 &+ 2A_1 A_2 \left(\frac{\pi}{l_g} \right)^2 \left(\frac{2\pi}{l_g} \right)^2 \int_0^{l_g} \sin \left(\frac{\pi x}{l_g} \right) \sin \left(\frac{2\pi x}{l_g} \right) dx + 2A_1 A_3 \left(\frac{\pi}{l_g} \right)^2 \left(\frac{3\pi}{l_g} \right)^2 \int_0^{l_g} \sin \left(\frac{\pi x}{l_g} \right) \sin \left(\frac{3\pi x}{l_g} \right) dx + \dots \\
 &= \frac{A_1^2 \pi^4}{l_g^4} \int_0^{l_g} \frac{1 - \cos \left(\frac{2\pi x}{l_g} \right)}{2} dx + \frac{A_2^2 2^4 \pi^4}{l_g^4} \int_0^{l_g} \frac{1 - \cos \left(\frac{4\pi x}{l_g} \right)}{2} dx + \dots + \frac{A_n^2 n^4 \pi^4}{l_g^4} \int_0^{l_g} \frac{1 - \cos \left(\frac{2n\pi x}{l_g} \right)}{2} dx + 0 \\
 &= \frac{A_1^2 \pi^4}{l_g^4} \frac{l_g}{2} + \frac{A_2^2 2^4 \pi^4}{l_g^4} \frac{l_g}{2} + \dots + \frac{A_n^2 n^4 \pi^4}{l_g^4} \frac{l_g}{2} \\
 &= \frac{\pi^4}{2l_g^3} \sum_{m=1}^n m^4 A_m^2
 \end{aligned}$$

Therefore:

$$\begin{aligned}
 \Pi &= \frac{E_g I_g}{2} \int_0^{l_g} \left(\frac{d^2\omega_1(x)}{dx^2} \right)^2 dx - \sum_{i=1}^{MN} \frac{1}{2} F_i \omega_1(x_i) \\
 &= \frac{E_g I_g \pi^4}{2 \cdot 2l_g^3} \sum_{m=1}^n m^4 A_m^2 - \frac{1}{2} \sum_{i=1}^{MN} \left(F_i \sum_{m=1}^n A_m \sin \frac{m\pi x_i}{l_g} \right) \quad (n \rightarrow \infty) \tag{5} \\
 &= \frac{E_g I_g \pi^4}{4l_g^3} \sum_{m=1}^n m^4 A_m^2 - \frac{1}{2} \sum_{i=1}^{MN} \left(F_i \sum_{m=1}^n A_m \sin \frac{m\pi x_i}{l_g} \right)
 \end{aligned}$$

where $F_i (i = 1, 2, \dots, MN)$ is the fastener force, E_g is the elastic modulus of the rail and I_g is the equivalent cross-sectional moment of inertia of the rail [24].

According to the Rayleigh Ritz method $\frac{\partial \Pi}{\partial A_m} = 0$, can be obtained:

$$\frac{E_g I_g \pi^4}{2l_g^3} m^4 A_m - \sum_{i=1}^{MN} F_i \sin \frac{m\pi x_i}{l_g} = 0 \tag{6}$$

Then, the following conclusion can be deduced from the above formula:

$$A_m = \frac{2l_g^3}{E_g I_g \pi^4 m^4} \sum_{i=1}^{MN} F_i \sin \frac{m\pi x_i}{l_g} \quad (m = 1, 2, \dots, n) \tag{7}$$

The above formulas can be arranged as follows:

$$\omega_1(x_j) = \sum_{i=1}^{MN} F_i \sum_{m=1}^n \frac{2l_g^3}{E_g I_g \pi^4 m^4} \sin \frac{m\pi x_i}{l_g} \sin \left(\frac{m\pi x_j}{l_g} \right) \quad (j = 1, 2, \dots, MN) \tag{8}$$

2.3.2. Girder Displacement

The mechanical model of the bridge is shown in Figure 3.

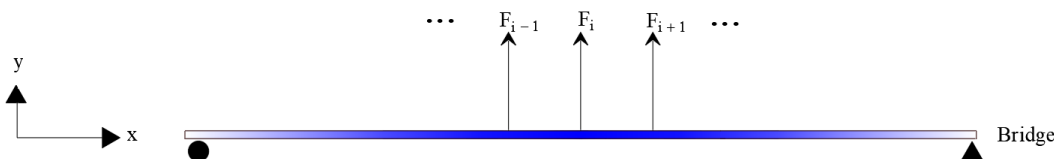


Figure 3. Mechanics model of the bridge.

If the k^{th} pier settles, the displacement function $\omega_{2,k,k}$ of the k^{th} span girder (the left span of the settlement pier) can be expressed as follows:

$$\omega_{2,k,k}(x) = \frac{x - k(l_l + s_l)}{l_l}d \tag{9}$$

The displacement function $\omega_{2,k,k+1}$ of the $(k + 1)^{th}$ beam (right span of the settlement pier) can be expressed as follows:

$$\omega_{2,k,k+1}(x) = \frac{(k + 2)l_l + (k + 1)s_l - x}{l_l}d \tag{10}$$

where l_l is the length of a single span, d is the settlement of the pier, and s_l is the girder space.

2.3.3. Analytic Expression of Mapping Relationship

Let k_s be the equivalent stiffness of the fastener, then the i^{th} fastener force can be expressed as:

$$F_i = k_s[\omega_2(x_i) - \omega_1(x_i)] \tag{11}$$

The fastener force is expressed in matrix form as follows:

$$\mathbf{F} = k_s(\mathbf{H} \cdot d - \mathbf{A} \cdot \mathbf{F}) \tag{12}$$

where: \mathbf{F} is the fastener force matrix; \mathbf{A} is the influence coefficient matrix of the fastener force on rail displacement; \mathbf{H} is the influence coefficient matrix of settlement on bridge displacement.

According to the Equations (12), the fastener force matrix can be expressed as a single value function of settlement:

$$\mathbf{F} = \left(\mathbf{A} + \frac{\mathbf{E}}{k_s} \right)^{-1} \mathbf{H} \cdot d \tag{13}$$

where \mathbf{E} is the identity matrix of the same dimension as \mathbf{A} [25].

The mapping deformation of the rail with the pier settlement can be obtained by substituting Equation (13) into Equation (8).

$$\mathbf{W}_1 = \mathbf{A} \left(\mathbf{A} + \frac{\mathbf{E}}{k_s} \right)^{-1} \mathbf{H} \cdot d \tag{14}$$

where: \mathbf{W}_1 is the rail displacement matrix of all fastener positions.

3. Analysis of Examples

In order to verify the accuracy of the analytical expressions, this paper selects two typical deformations: the pier settlement and the girder vertical fault. SAM, FAM [26], and AFEM were used to calculate the mapping relationship curve of the rail with girder deformation.

First of all, based on ANSYS finite element software, an AFEM of 6-span-32 m simply supported bridge CRTS III SBT system was established. The rails, track slabs, girder, and bridge piers are all simulated by BEAM 3 elements. Fasteners, SCCFL, and bearing are simulated by COMBINE 14 spring elements. The material properties of each component are shown in Table 1. Secondly, the corresponding forced displacement (the pier settlement and the girder vertical fault) is applied to the bridge structure, the displacement convergence criterion is defined as 0.05, and the sub-step is defined as the automatic time step. Ultimately, the static analysis is carried out.

Table 1. The materials and properties of the bridge and CRTS III SBT system.

Components	Materials	Height/mm	Elastic Modulus/GPa	Poisson’s Ratio	Vertical Spring Stiffness/(N/m)
Rail	U71Mn(K)	176	206	0.3	-
Fasteners	WJ-8C	38	-	-	3.5×10^7
Track slab	C60 concrete	200	36	0.2	-
Filling layers	C40 SCC	90	32.5	0.2	1.8×10^9
Base slab	C40 concrete	200	32.5	0.2	-
Girder	C50 concrete	3050	34.5	0.2	-

According to the mapping relationship between bridge vertical deformation and geometrical morphology of the rail surface, the program of the mapping relationship is compiled by using the MATLAB software (R2018a version from MathWorks, USA). The calculation processes of the SAM and the FAM are shown in Figure 4. The main parameters of the two models are as follows: the span length and span number of the simply supported bridge are consistent with AFEM; the length of both ends of the subgrade section is a single span length; the beam spacing is 20 mm; the track slab spacing is 70 mm, and other parameters are consistent with Table 1.

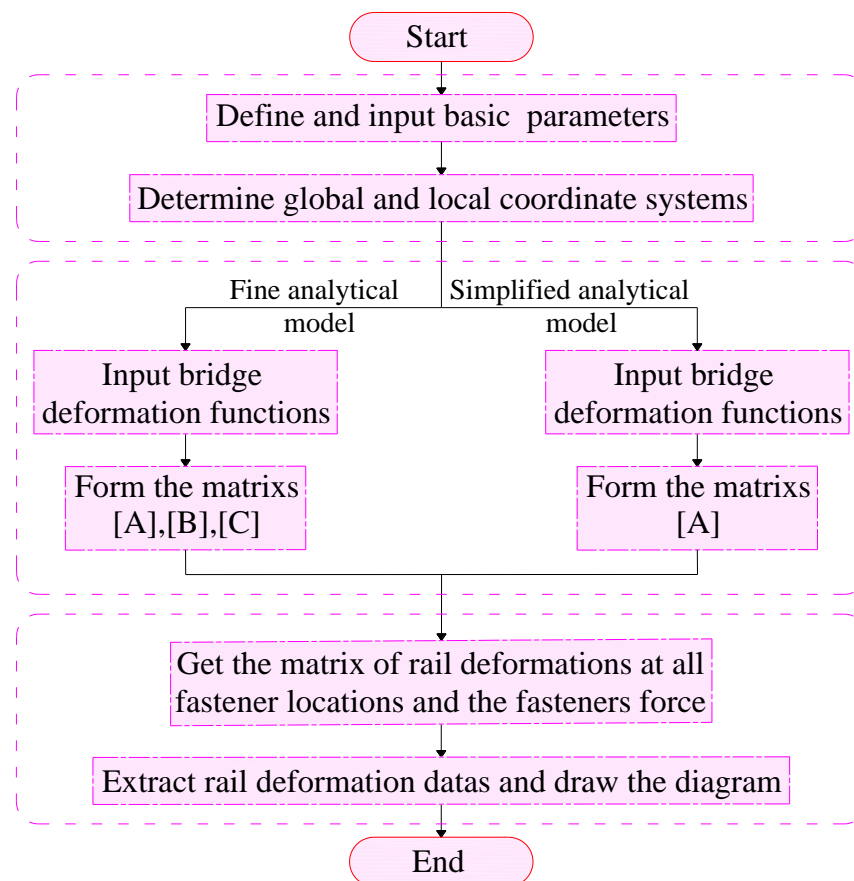


Figure 4. Cont.

```

ks = 1/(3.5 × 107); % Vertical stiffness of fasteners
X = xlsread('local coordinates of girder deformation.xlsx', 'A2:A417');
x = xlsread('overall coordinates of fastener position.xlsx', 'A2:A417');
Gn = 8; % Girder number
M = 52; % 52 fasteners on a girder
MN = M·Gn; % Total number of fasteners
L = 32.6; % Girder length
Gap = 0.02; % Girder gap
Lg = L·Gn + Gap·(Gn-1); % Total length of rails
Eg = 2.06 × 1011; % Elastic modulus of rails
Ig = 3.217 × 10-5; % Moment of inertia of rails
n = 1000; % Number of iterations
Pi = 3.14159
A = zeros(MN,MN); % Define the A matrix
E = eye(MN,MN); % Define the E matrix

for i = 1:MN
    for j = 1:MN
        for m = 1:n
            A(i, j) = A(i, j) + 2 × (lg^3/(Eg·Ig·pi^4·m^4)) · sin(m·pi·x(i)/lg) · sin(m·pi·x(j)/lg);
        end
    end
end

A;
F = inv(A·ks·E) · X;
W = A·F;
plot(W)
    
```

Figure 4. MATLAB flowchart and code for SAM and FAM.

3.1. Mapping Relationship between Pier Settlement and Rail Deformation

According to the limit value of girder deformation, the pier settlement is set as 5 mm, as shown in Figure 5. Case 1: the settlement of pier 3 is 5 mm. Case 2: the settlement of pier 2 is 5 mm and that of pier 3 is 3 mm. Case 3: the settlement of pier 2 is 5 mm and that of pier 4 is 3 mm.

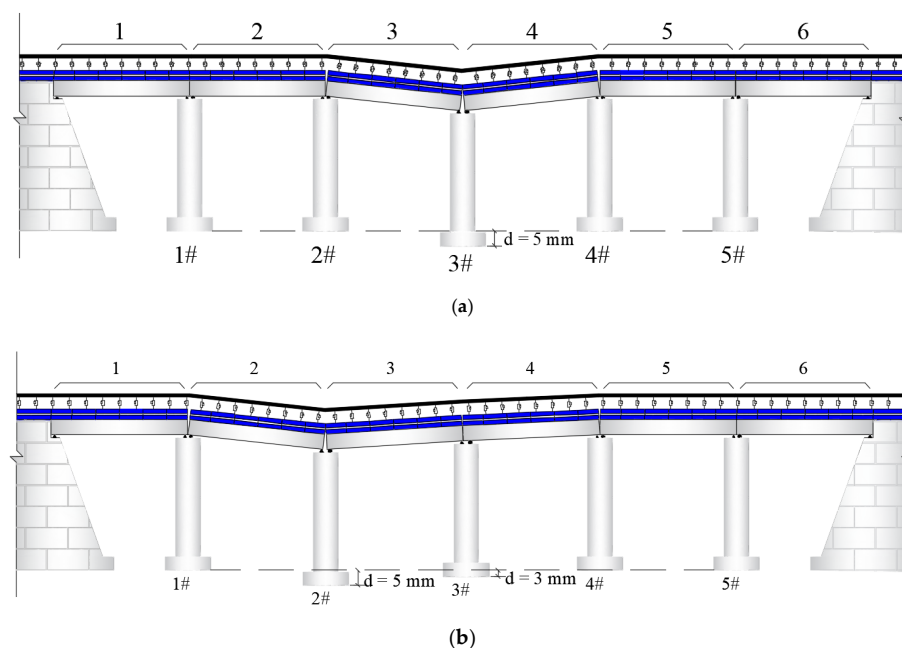


Figure 5. Cont.

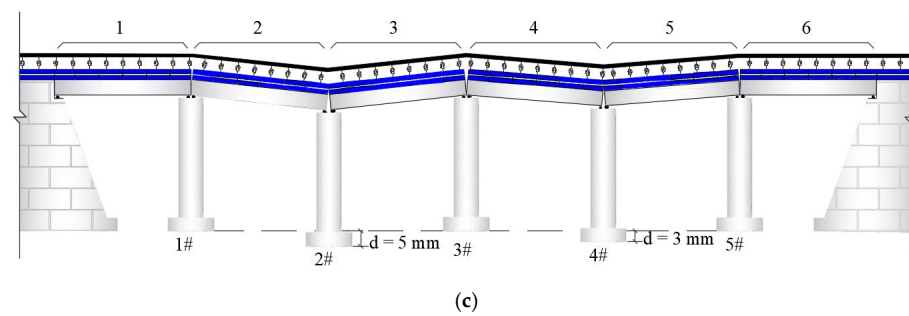


Figure 5. Deformation diagram of the bridge during pier settlement. (a) The settlement of a single pier. (b) The uneven settlement of two adjacent piers. (c) The uneven settlement of two separated piers.

The mapping deformation curve of a rail with a pier settlement calculated by the three models is shown in the Figure 6. It can be seen that in the three cases, the peak value of the mapping deformation curve obtained by AFEM is slightly larger than that of the SAM and FAM, but the difference between the three peak values is no more than 1%, which shows that the SAM is in good agreement with the AFEM and FAM, indicating that the three models can be used to calculate the mapping deformation of the rail with the pier settlement, and the correctness of the SAM is demonstrated. In the settlement area, the rail deformation occurs with the pier settlement; when far away from the settlement area, the rail deformation decreases in the form of microwave; when in and out of the settlement area, the rail slightly upwarps; at the settlement pier location, the rail mapping deformation has a gentle and continuous transition curve; and the peak value of the rail deformation curve obtained by the three models is slightly less than that of the pier settlement. Compared with the three models, the SAM has certain advantages. It can not only directly describe the factors affecting rail deformation, but also clearly expresses the relationship between each factor and rail deformation. Further saving the modeling time of ANSYS.

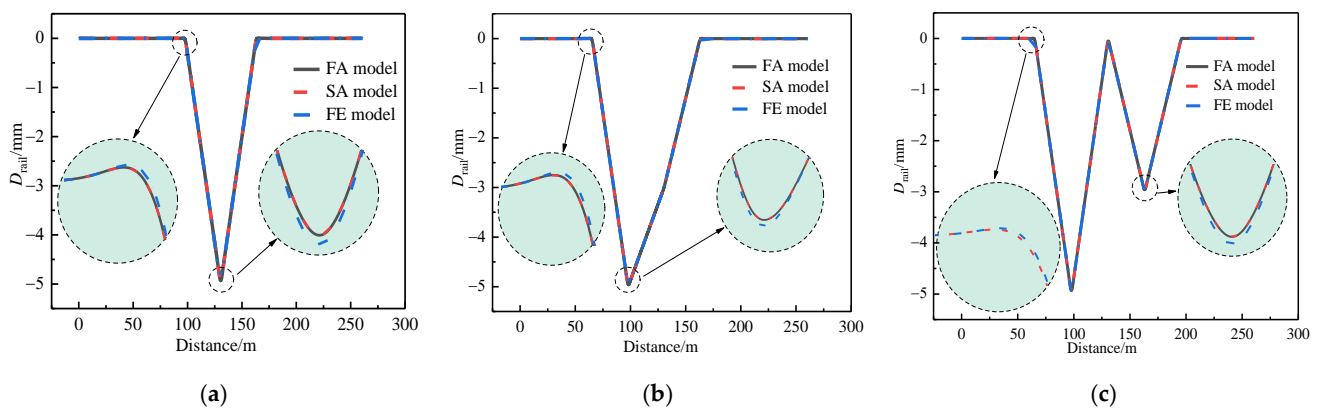


Figure 6. Mapping deformation of the rail with the pier settlement. (a) The #3 pier settlement; (b) #2 and #3 pier settlement; and (c) the #2 and #4 pier settlement.

3.2. Mapping Relationship between Girder Vertical Fault and Rail Deformation

According to the provision of the girder vertical fault, the girder vertical fault value is set as 3 mm, as shown in Figure 7. Case 1: the vertical fault value of the third girder is 3 mm. Case 2: the vertical fault value of the third girder is 3 mm, and the vertical fault value of the fifth girder is 2 mm.

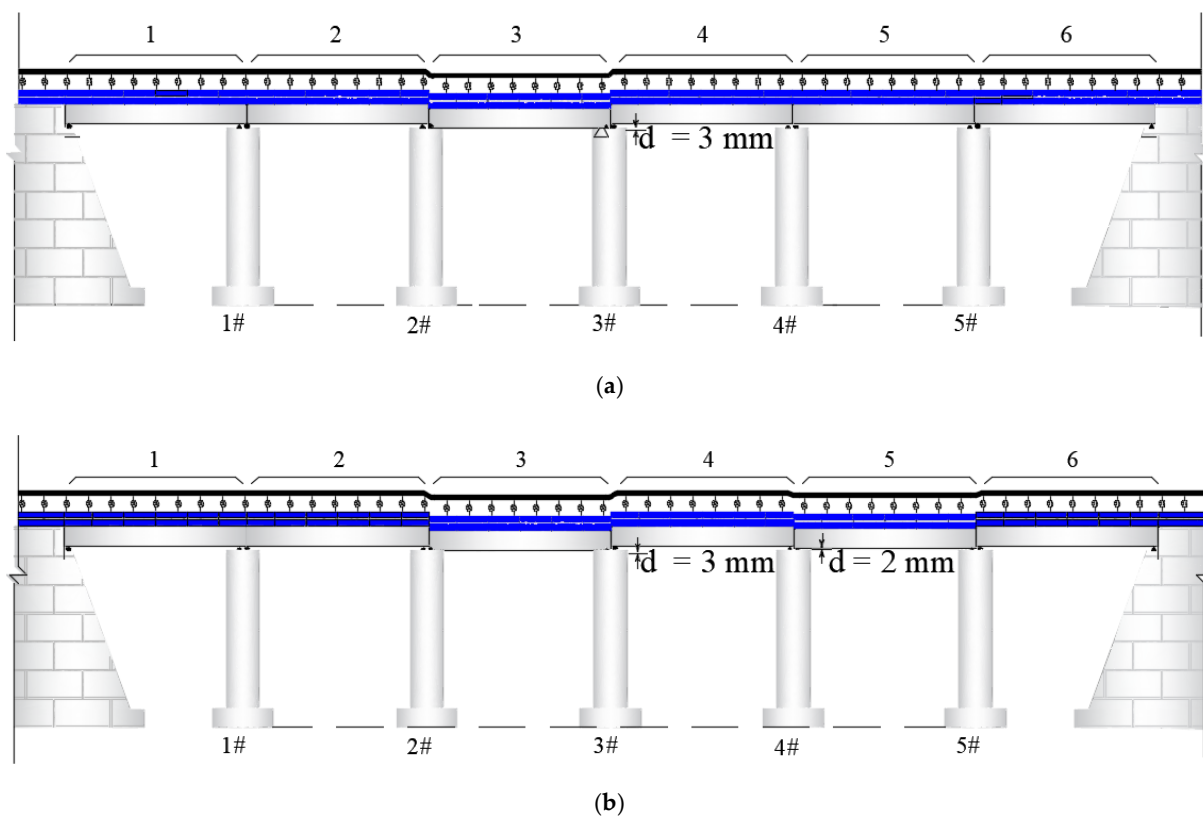


Figure 7. Deformation diagram of bridge under vertical girder fault. (a) The vertical fault of the single girder. (b) The uneven vertical fault of two separated girders.

The mapping deformation curves of the rail with the girder vertical fault calculated by the three models are shown in Figure 8. It can be seen that under the two cases, the rail mapping deformation curves calculated by the three models basically coincide. The downward deformation peak values of the rail of the AFEM is larger than that of the FAM, and that of the SAM is the minimum. The difference between the three peak values is not more than 1%. This shows that the rail deformation curve obtained by the SAM is relatively safe, and proves the practicability of the SAM under the condition of girder vertical fault. Due to the girder vertical fault, the rail has a significant deformation. It can be seen from Figure 8a that the rail mapping deformation curve has symmetry when the single girder has vertical fault. It can be seen from Figure 8b that the overall rail mapping deformation curve is asymmetric when the girder vertical fault occurs between two separated girders. However, the rail deformation curve within the area of the deformation girder still has symmetry. Outside the area of the deformation girder, the rail deformation rapidly decreases until it is zero. When in and out of the girder deformation area, the rail mapping deformation curve presents upward warping and a downward concave phenomenon, which will have adverse effects on the driving safety and riding comfort of a high-speed train. In the area of the girder vertical fault, the rail deformation increases rapidly, and the maximum of the rail deformation is slightly less than the maximum of the girder vertical fault, but the rail deformation curve is generally consistent with the girder vertical fault deformation curve.

Through the verification of pier settlement and girder vertical fault, it can be seen that the rail deformation curves obtained by SAM and FAM are almost identical and slightly smaller than AFEM, which fully shows that the simplified analytical solution can achieve high accuracy. The reason why the simplified analytical solution can reach the precision of the fine analytical solution is that the SCCFL is equivalent to winker linear springs distributed uniformly along the center line of the rail in the fine analytical solution. In fact, due to the high strength of the SCCFL, when the girder undergoes linear deformation, because of the large equivalent spring stiffness, the spring hardly deforms. Additionally,

because the connection between the base slab and the girder is strong, this paper regards the CRTS III SBT system as a composite plate. Therefore, this paper assumes that the deformation of the CRTS III SBT system and the girder is coordinated. The simplified analytical solution derived has higher accuracy, less parameters involved, more convenient calculation, and efficiency.

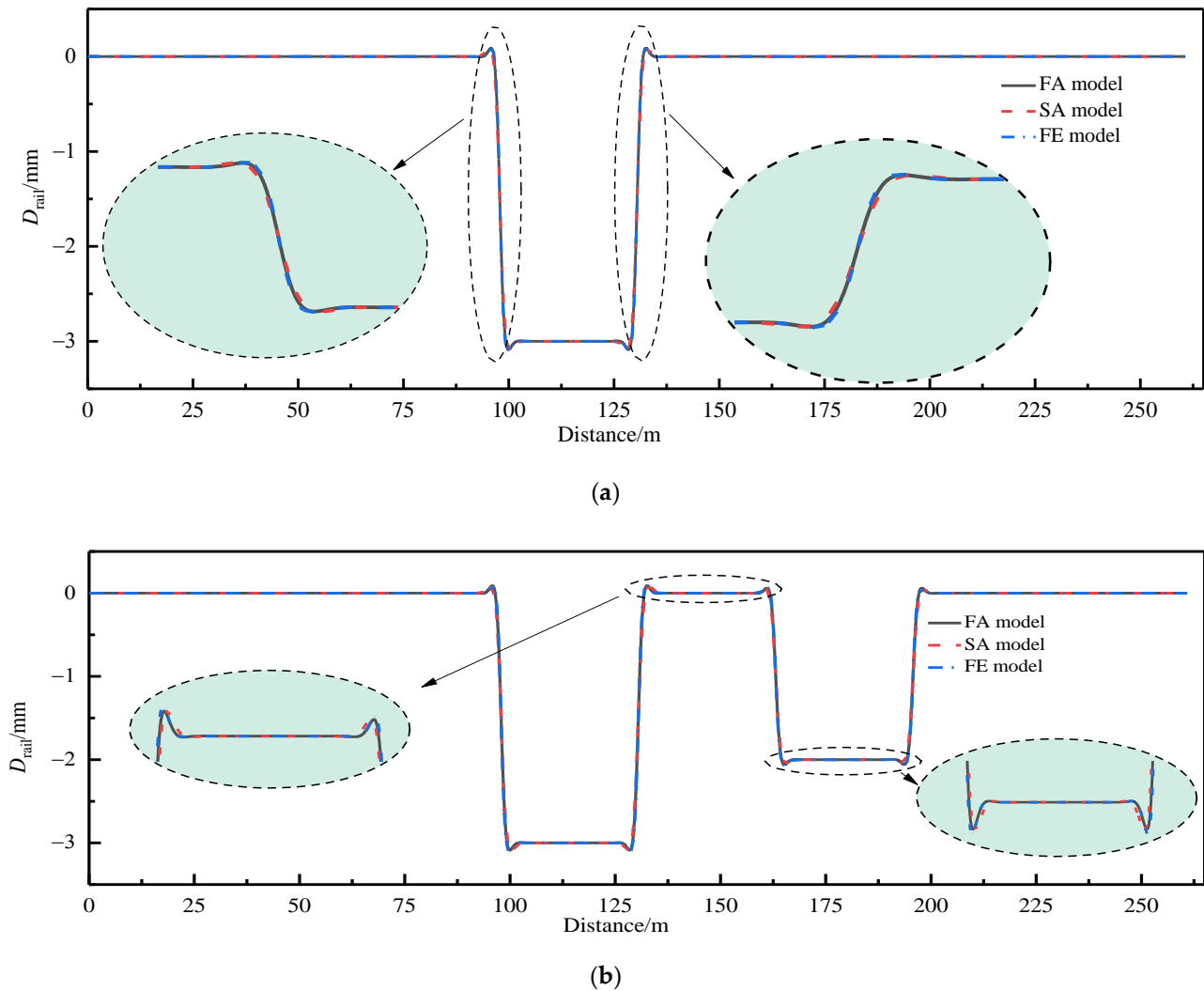


Figure 8. Mapping deformation of the rail under the vertical girder fault. (a) third girder vertical fault of 3 mm; (b) third girder vertical fault of 3 mm and fifth girder vertical fault of 2 mm.

4. Influencing Factors of Rail Deformation

4.1. The Influence of Pier Settlement Amplitudes on Rail Deformation

According to the verified SAM of the mapping relationship between girder deformation and rail deformation, the key factors affecting the bridge–rail mapping relationship can be summarized as pier settlement, bridge span, settlement type, and fastener stiffness. Based on the verified SAM, the influence of key parameters, such as pier settlement, fastener stiffness, bridge span, and girder vertical fault amplitude on rail mapping deformation is studied.

Taking the 6-span 32 m simply supported bridge model as an example, without changing the structure and parameter of bridge, subgrade, and CRTS III SBT, the verified SAM is used to calculate the settlement of pier #3 with 3 mm, 5 mm, 10 mm, 15 mm, and 20 mm, respectively, and the calculation results of the rail mapping deformation curve and the fastener internal force under different pier settlement amplitudes are obtained. It can be seen in Figure 9.

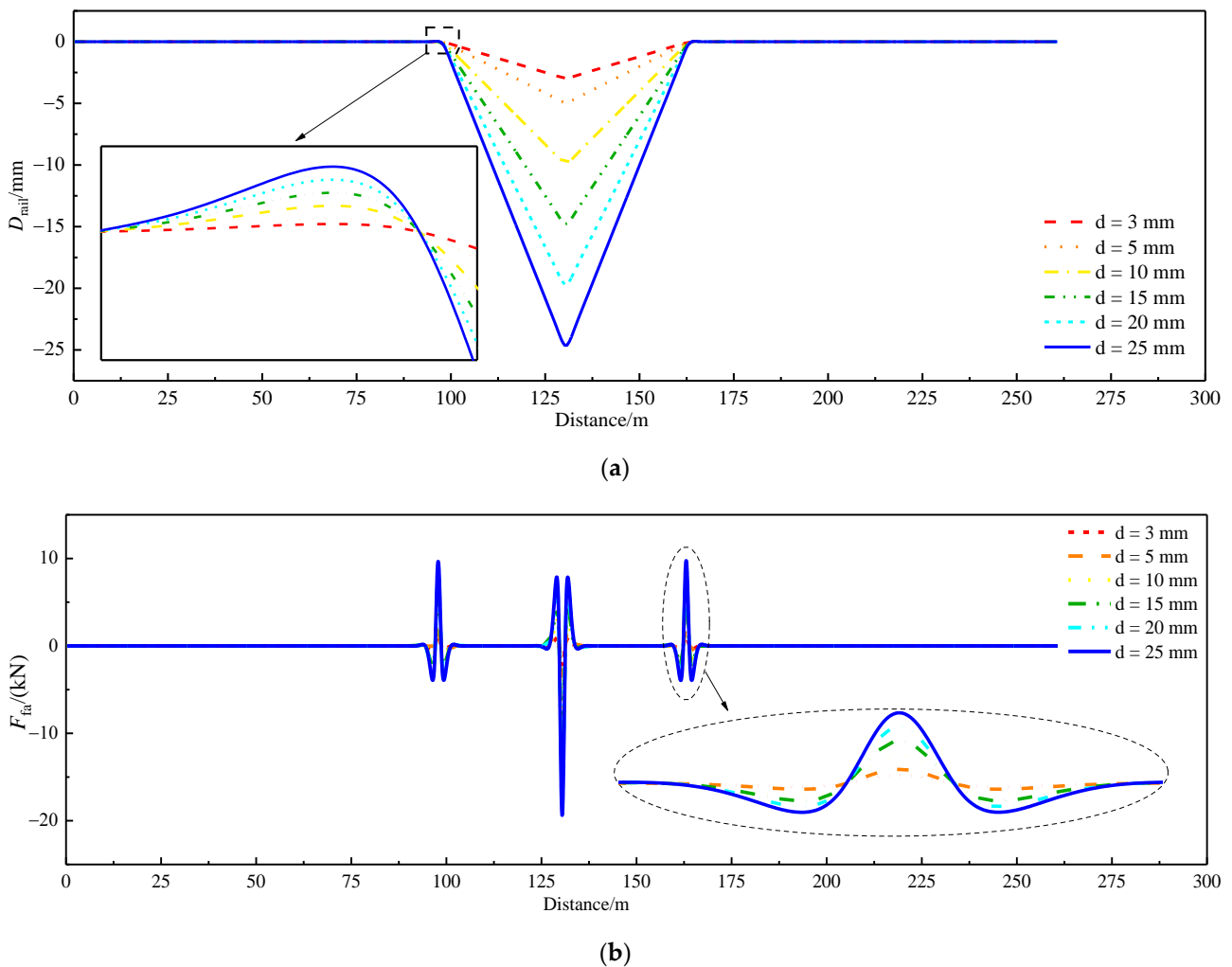


Figure 9. The influence of pier settlement amplitudes. (a) Mapping deformation of the rail under different pier settlements. (b) Fastener force under different pier settlements.

From Figure 9a, it can be seen that when the pier settlement is different, the shape of the rail mapping deformation curve with the pier settlement is similar. The greater the pier settlement is, the greater the rail mapping deformation amplitude is in the settlement area, the more obvious the upward warping degree of the rail mapping deformation curve is in and out of the settlement area, and the greater the “bending angle” formed.

It can be seen from Figure 9b that when the pier settlement with different amplitudes occurs, the curve of the fastener force is similar [27]. The fastener force amplitude increases with the increase in the pier settlement amplitude. At the settlement pier and its two adjacent piers, the fastener force changes dramatically. The fastener force amplitude at the settlement pier is slightly larger than that of the adjacent pier, and the fastener force amplitude at the two adjacent piers is similar. At the two adjacent piers, the girder on both sides of the settlement pier is upward warped, resulting in the rail bulge deformation at the adjacent pier, so the direction of the fastener force at the adjacent pier position and the settlement pier position is opposite.

The area where the rail deformation exceeds 0.001 mm is defined as the rail mapping deformation area. When the ratio of rail mapping deformation amplitude (the sum of positive amplitude and negative amplitude) to the length of the rail mapping deformation area is defined as the rail unevenness, then the rail unevenness can be expressed as:

$$R_r = \frac{D_+ + D_-}{L_r} \tag{15}$$

In the Equation (15), D_+ represents the rail positive mapping deformation amplitude(m); D_- represents the rail negative mapping deformation amplitude(m); L_r represents the rail mapping deformation area length(m); and R_r represents the rail unevenness.

The rail mapping deformation area length and rail unevenness are shown in Table 2. The relationship between the rail mapping deformation amplitude, deformation area length and rail unevenness, and settlement amplitude of the bridge pier is shown in Figure 10. As can be seen from Figure 10, with the increasing settlement amplitude of the bridge pier, the length of the rail mapping deformation area increases continuously, the rail unevenness increases gradually, and the mapping deformation amplitude of rail positive and negative increases linearly [28]. It means that when the bridge pier settlement deformation is too large, it will seriously affect the safety and smoothness of train operation.

Table 2. Rail mapping deformation area length and rail unevenness of pier settlement.

Settlement Amplitude of Pier (mm)	Girder Length (m)	Rail Positive Mapping Deformation Amplitude D_+ (m)	Rail Negative Mapping DeformationAmplitude D_- (mm)	Rail Mapping Deformation Area Length L_r (m)	Rail Unevenness R_r
3	32	2.961	0.004	70.800	0.042
5	32	4.935	0.006	71.000	0.070
10	32	9.869	0.013	71.200	0.139
15	32	14.804	0.019	71.400	0.208
20	32	19.738	0.026	71.600	0.276
25	32	24.700	0.031	71.800	0.344

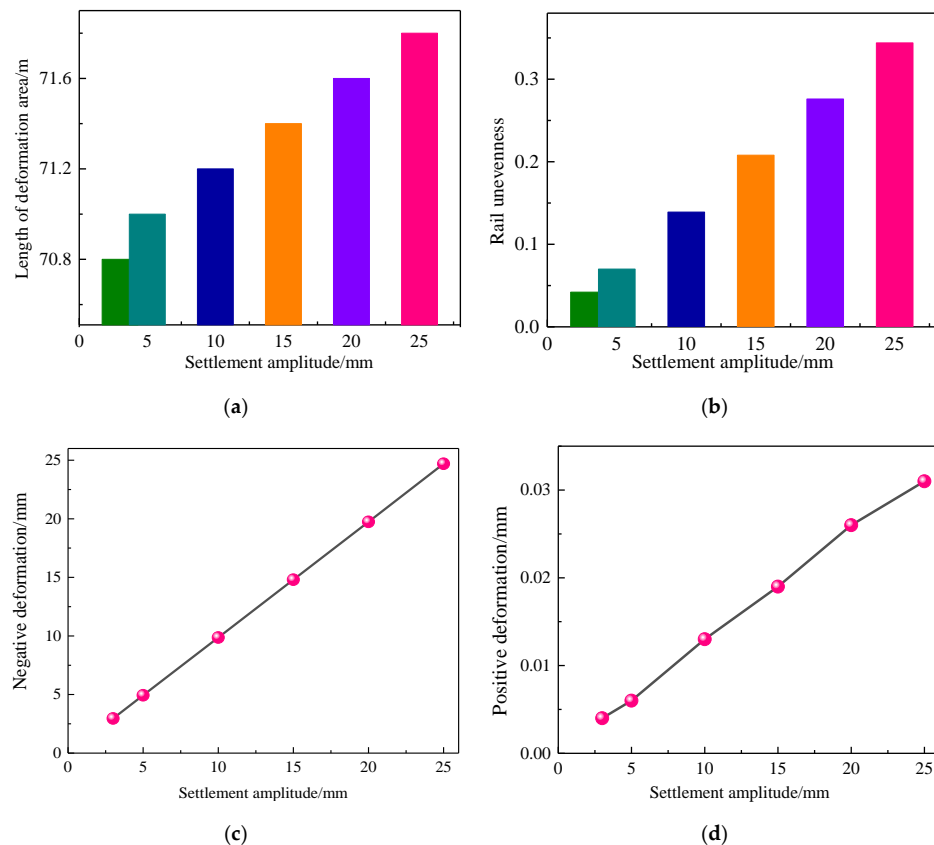


Figure 10. Relationship between rail mapping deformation amplitude, deformation area length and rail unevenness, and settlement amplitude of the bridge pier. (a) Length of the deformation area; (b) rail unevenness; (c) positive deformation; and (d) negative deformation.

4.2. The Influence of Fastener Stiffness on Rail Deformation

As an important joint structure, a fastener has a great influence on rail deformation. Therefore, this paper still takes the 6-span 32.6 m simply supported bridge model as an example to study the influence of fastener stiffness on rail mapping deformation. Without changing the structure and parameter values, when the 5 mm settlement occurs for pier #3, the SAM is used to calculate the mapping deformation curve of the rail under 5 fastener stiffness (10 kN/mm, 25 kN/mm, 35 kN/mm, 45 kN/mm, and 55 kN/mm). The mapping deformation curve of the rail is shown in Figure 11a and the variation curve of the fastener internal force is shown in Figure 11c.

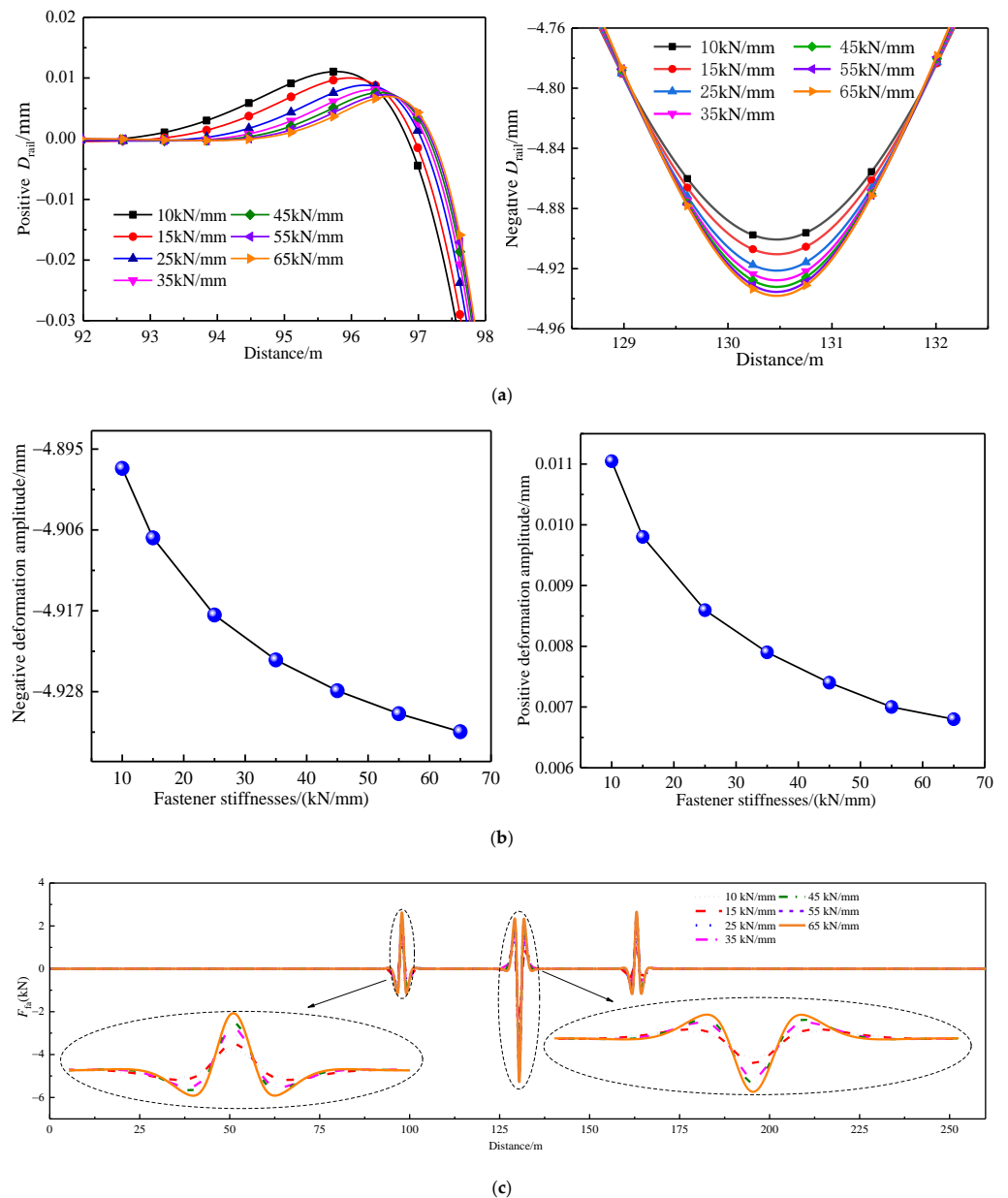


Figure 11. The influence of fastener stiffness. (a) Mapping deformation of the rail under different fastener stiffnesses; (b) mapping deformation amplitude of the rail under different fastener stiffnesses; and (c) fastener force under different fastener stiffnesses.

It can be seen from Figure 11a that the fastener stiffness is different and the shape of rail mapping deformation curve is generally consistent when 5 mm settlement occurs at pier #3. It can be seen from Figure 11b that at the critical point in and out of the settlement

area [29], with the increase in fastener stiffness, the positive deformation amplitude of the rail gradually decreases. At the pier settlement, with the increase in fastener stiffness, the negative deformation amplitude of the rail gradually increases. From Figure 11c, it can be seen that the shape of the fastener internal force curve is generally consistent, which fully shows that the rail mapping deformation has a good follow-up with the settlement of the pier [30]. In conclusion, with the increase in the fastener stiffness, the fastener internal force increases, the rail mapping deformation also increases, and the length of the rail mapping deformation area decreases gradually, which fully shows that the smaller the fastener vertical stiffness is, the smoother the mapping deformation curve of the rail is. From this conclusion, it can be concluded that the track–bridge system with low stiffness fasteners is more conducive to resist the influence of pier settlement within a reasonable range.

4.3. The Impact of the Girder Span Length on Rail Deformation

In order to study the influence of the girder span length on rail mapping deformation and fastener internal force, this study uses the 6-span simply supported bridge model with a girder span length of 16 m, 20 m, 24 m, and 32 m as an example. Without changing the structure and parameter values, the rail mapping deformation curve and fastener internal force curve were calculated by using the verified SAM when the #3 pier has five different settlements of 3 mm, 5 mm, 10 mm, 15 mm, and 20 mm. The calculation results are shown in Figure 12.

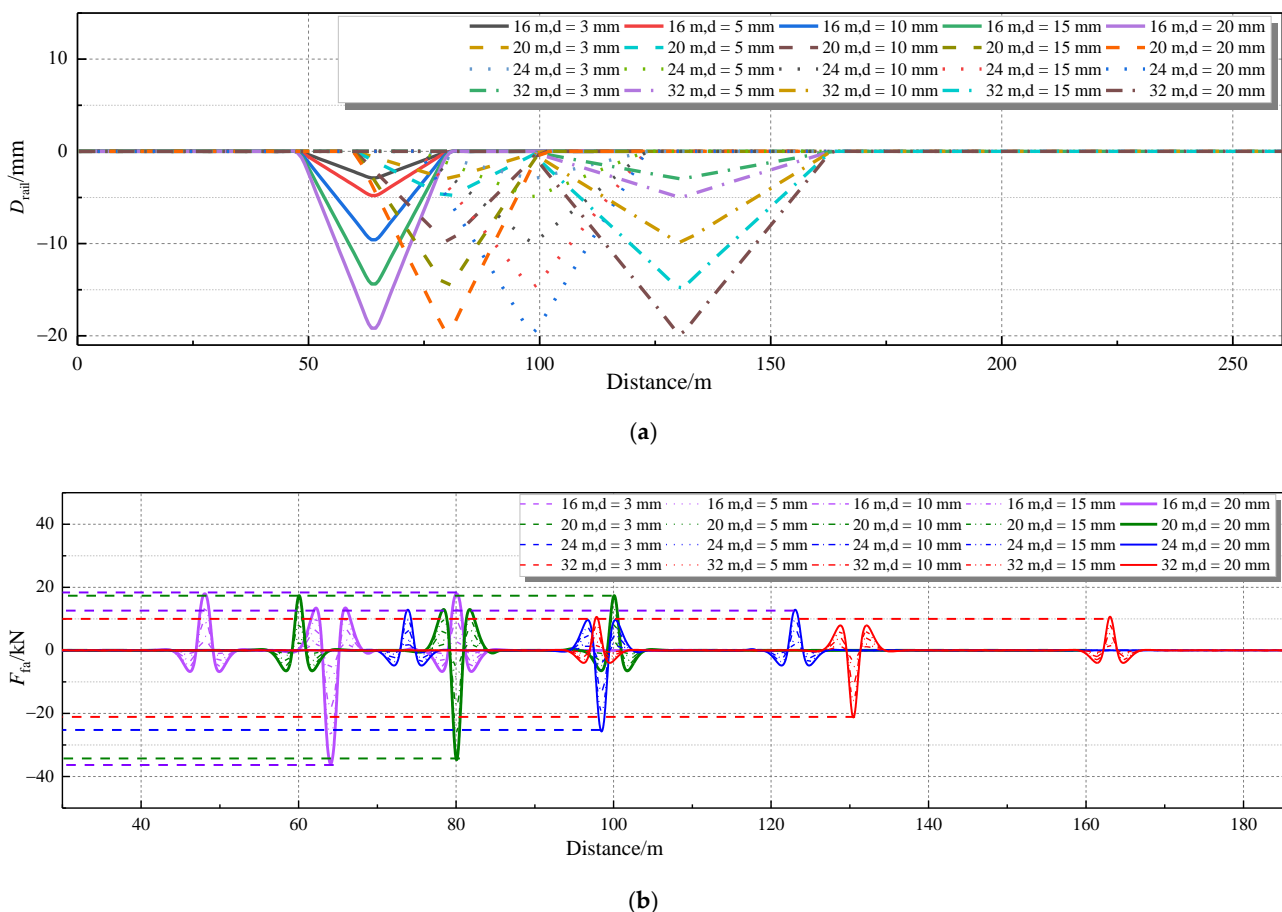


Figure 12. The influence of girder span length. (a) Rail deformation of simply supported bridges with different span lengths. (b) Fastener stiffness of simply supported bridges with different span lengths.

It can be seen from Figure 12 that when the pier settlement is within the range of 3–20 mm [31], the increase in girder span length has no obvious effect on the rail mapping deformation. When the same pier settlement occurs for a different girder span length, the

upward deformation amplitude of the rail at the adjacent pier’s position decreases with the increase in girder span length. That is to say, the upward deformation amplitude of the rail at the adjacent pier position of the 16 m span simply supported bridge is the largest, and the upward deformation amplitude of the rail at the adjacent pier position of the 32 m span simply supported bridge is the smallest. The results show that, with the increase in girder span, the bending angle of the adjacent pier position caused by pier settlement is smaller, and the influence on the track–bridge system is smaller. With the increase in girder span length, the change in the rail mapping deformation curve at the settlement pier position is not obvious. That is to say, under the condition of pier settlement, the following deformation capacity of rail is better. It can be seen from Figure 12 that when the bridge pier settlement is within the range of 3–20 mm [31], the increase in girder span length has a significant impact on the fastener internal force. When the same pier settlement occurs in different girder span length, with the increase in girder span length, the fastener internal force at the settlement pier position and adjacent pier position decreases significantly, which indicates that with the decrease in girder span length, the influence of pier settlement on the track–bridge system will be greater.

4.4. The Impact of the Girder Vertical Fault Amplitudes on Rail Deformation

In order to study the influence of the girder vertical fault on rail mapping deformation, a 6-span 32 m simply supported bridge is taken as an example. Without changing the structure and parameter values, the verified SAM is used to calculate the girder vertical fault when the girder vertical fault deformation is 0.5 mm, 1.0 mm, 2.0 mm, 3.0 mm, 4.0 mm, and 5.0 mm [32]. The results are shown in Figures 13 and 14. The rail mapping deformation area length and rail unevenness are shown in Table 3.

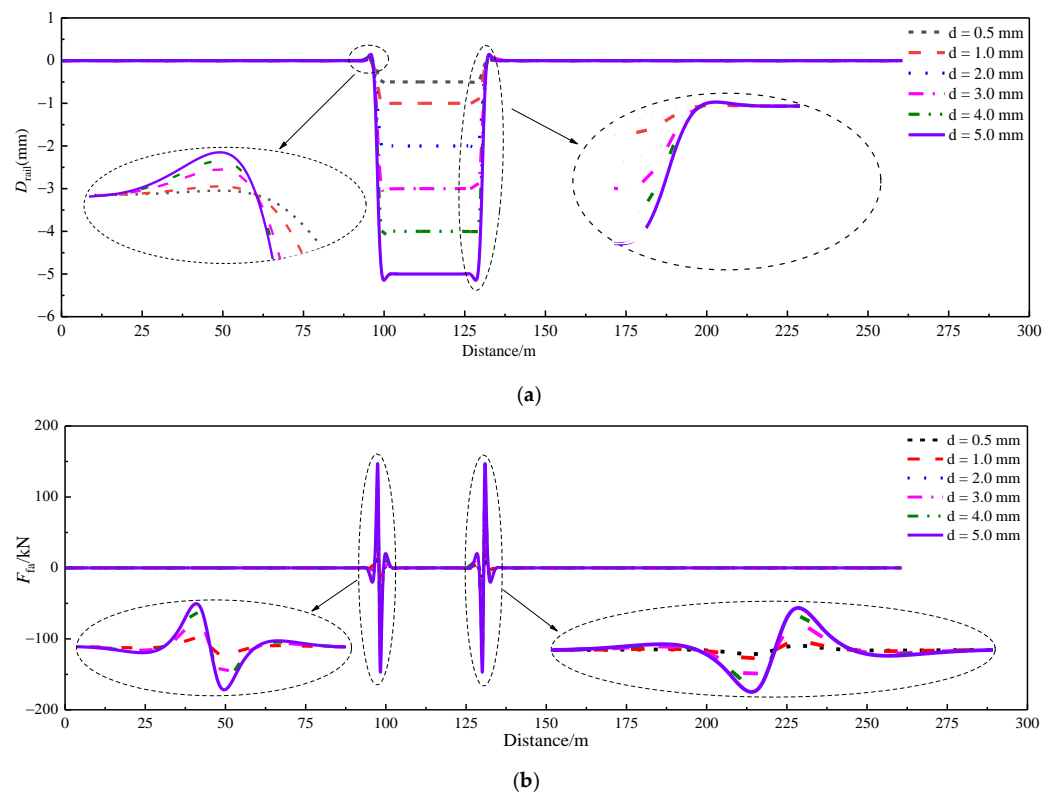


Figure 13. The influence of the girder vertical fault. (a) Rail deformation under different amplitudes of vertical girder fault; (b) fastener force under different amplitudes of vertical girder fault.

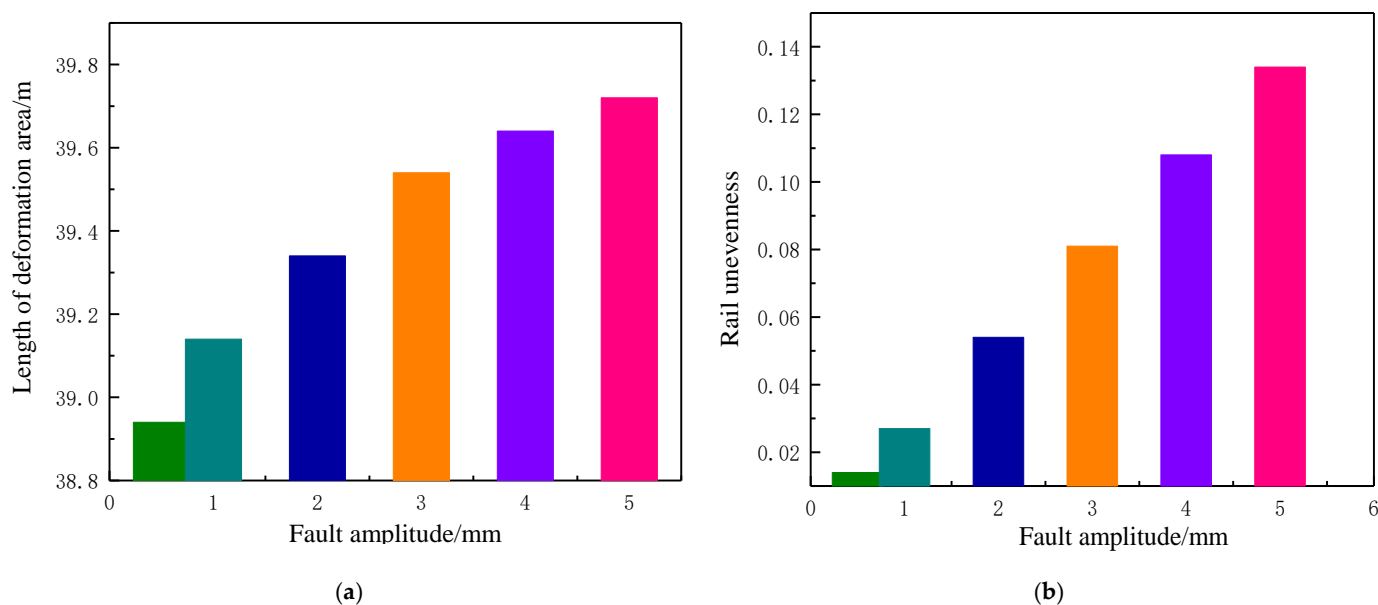


Figure 14. Relationship between length of deformation area and rail unevenness and fault amplitude of the girder. (a) Length of deformation area; (b) rail unevenness.

Table 3. Rail mapping deformation area length and rail unevenness of girder vertical fault.

Fault Amplitude (mm)	Girder Length (m)	Rail Positive Mapping Deformation Amplitude D_+ (m)	Rail Negative Mapping Deformation Amplitude D_- (mm)	Rail Mapping Deformation Area Length L_r (m)	Rail Unevenness R_r
0.5	32	0.016	0.516	38.94	0.014
1	32	0.033	1.033	39.14	0.027
2	32	0.066	2.066	39.34	0.054
3	32	0.099	3.099	39.54	0.081
4	32	0.132	4.132	39.64	0.108
5	32	0.165	5.165	39.72	0.134

From Figure 13a, it can be seen that the geometry of the rail mapping deformation curve is the same under different girder vertical fault conditions, and the rail mapping deformation geometry and girder deformation shape always keep a good follow-up in the girder vertical fault area. With the increase in vertical fault value, the amplitude of rail mapping deformation in the vertical fault deformation area also increases, and the more obvious the rail upward warping and downward concave phenomenon when in and out of the vertical fault deformation area. It can be seen from Figure 13b that the shape of the fastener internal force curve is consistent when the value of the vertical fault deformation is different, which mainly concentrates on both sides of the girder seam center line at both ends of the girder where the vertical fault occurs. The amplitude of the fastener internal force and the corresponding rail deformation increases significantly with the increase in vertical fault value. It can be seen from Table 3 that with the increase in fault amplitude, the amplitude of upward and downward rail deformation increases [33]. It can be seen from Figure 14a that with the increase in fault amplitude, the length of deformation area increases. It can be seen from Figure 14b that with the increase in fault amplitude, the rail unevenness increases [34].

5. Conclusions

The analytical solution of the mapping relationship between girder deformation and rail deformation in the CRTS III SBT multi-span simply supported bridge system is derived and verified. The influence of key parameters, such as pier settlement, fastener stiffness,

girder span length, and girder vertical fault on rail mapping deformation is studied, and the results are as follows:

- (1) The mapping deformation of the rail calculated by SAM, FAM, and AFEM is basically consistent, which proves the correctness of SAM in this paper. Compared with the AFEM, the SAM can better describe the key parameters affecting the rail deformation, save the modeling time of ANSYS, and improve the calculation efficiency.
- (2) The mapping deformation geometry of rails is different for different girder deformation modes. The mapping deformation geometry of rails has good “followability” and the mapping deformation geometry of rails depends on the girder deformation mode.
- (3) The mapping deformation amplitude of rails (maximum and minimum values) and the deformation amplitude of girders are positively linearly correlated; the positive deformation amplitude of rails gradually decreases with the increase in fastener stiffness, and the negative deformation amplitude gradually increases with the increase in fastener stiffness. The influence of girder length on the mapping deformation amplitude of rails is not obvious.
- (4) The length of mapping deformation area increases with the increase in girder deformation amplitude, and all of them are slightly larger than the length of two girders. The rail unevenness increases significantly with the increase in girder deformation amplitude.
- (5) The internal force of the fastener is mainly concentrated on girder gap, with abrupt changes at the starting position of the girder deformation and symmetry. The amplitude of the internal force of the fastener is positively correlated with the amplitude of the girder deformation and the fastener stiffness, and negatively correlated with the girder length. The shape of the rail mapping deformation curve is related to the shape of the internal force curve of the fastener.

Author Contributions: Formal analysis, X.L.; Methodology, Y.F.; Resources, L.J.; Writing – original draft, L.L.; Editing, W.Z. All authors have read and agreed to the published version of the manuscript.

Funding: The research was funded by the National Natural Science Foundation of China (51778630, U1934207, 52078487), Hunan Innovative Provincial Construction Project (2019RS3009).

Institutional Review Board Statement: Not applicable.

Informed Consent Statement: Not applicable.

Data Availability Statement: Not applicable.

Conflicts of Interest: The authors declare no conflict of interest.

References

1. Zhou, W.; Nie, L.; Jiang, L.; Feng, Y.; Tan, Z.; Chai, X. Mapping relation between pier settlement and rail deformation of unit slab track system. *Structures* **2020**, *27*, 1066–1074. [[CrossRef](#)]
2. Liu, L.; Jiang, L.; Zhou, W.; Peng, D.; Liu, X. Investigation of the seismic performance of CRTS III slab ballastless track of high-speed railway under low-cycle reciprocating load. *Soil Dyn. Earthq. Eng.* **2022**, *161*, 107432. [[CrossRef](#)]
3. Liu, L.; Jiang, L.; Zhou, W.; Yu, J.; Peng, K.; Zuo, Y. Study on the restoring force model for the high-speed railway CRTS III Slab Ballastless Track. *Arch. Civ. Mech. Eng.* **2022**, *22*, 148. [[CrossRef](#)]
4. Cui, C.; Feng, F.; Meng, X.; Liu, X. Fatigue Life Assessment of Intercity Track Viaduct Based on Vehicle–Bridge Coupled System. *Mathematics* **2022**, *10*, 1663. [[CrossRef](#)]
5. Sysyn, M.; Przybylowicz, M.; Nabochenko, O.; Kou, L. Identification of Sleeper Support Conditions Using Mechanical Model Supported Data-Driven Approach. *Sensors* **2021**, *21*, 3609. [[CrossRef](#)]
6. Sysyn, M.; Gerber, U.; Nabochenko, O.; Dehne, S. A Laboratory Study of Pressure Distribution and Residual Settlements in Wide Grading Double Layer Railway Ballast under Long-Term Cyclic Loading. *Arch. Civ. Eng.* **2020**, *66*, 561–578. [[CrossRef](#)]
7. Sysyn, M.; Przybylowicz, M.; Nabochenko, O.; Liu, J. Mechanism of Sleeper–Ballast Dynamic Impact and Residual Settlements Accumulation in Zones with Unsupported Sleepers. *Sustainability* **2021**, *13*, 7740. [[CrossRef](#)]
8. Sysyn, M.; Kovalchuk, V.; Nabochenko, O.; Kovalchuk, Y.; Voznyak, O. Experimental Study of Railway Trackbed Pressure Distribution Under Dynamic Loading. *Balt. J. Road Bridg. Eng.* **2019**, *14*, 504–520. [[CrossRef](#)]
9. Ntotsios, E.; Thompson, D.J.; Hussein, M.F. A comparison of ground vibration due to ballasted and slab tracks. *Transp. Geotech.* **2019**, *21*, 100256. [[CrossRef](#)]

10. Jiang, L.; Liu, X.; Xiang, P.; Zhou, W. Train-bridge system dynamics analysis with uncertain parameters based on new point estimate method. *Eng. Struct.* **2019**, *199*, 109454. [[CrossRef](#)]
11. Lazorenko, G.; Kasprzhitskii, A.; Khakiev, Z.; Yavna, V. Dynamic behavior and stability of soil foundation in heavy haul railway tracks: A review. *Constr. Build. Mater.* **2019**, *205*, 111–136. [[CrossRef](#)]
12. Varandas, J.; Paixão, A.; Fortunato, E.; Coelho, B.Z.; Hölscher, P. Long-term deformation of railway tracks considering train-track interaction and non-linear resilient behaviour of aggregates—A 3D FEM implementation. *Comput. Geotech.* **2020**, *126*, 103712. [[CrossRef](#)]
13. Galvín, P.; Romero, A.; Domínguez, J. Fully three-dimensional analysis of high-speed train-track-soil-structure dynamic interaction. *J. Sound Vib.* **2010**, *329*, 5147–5163. [[CrossRef](#)]
14. Ju, S.H. 3D analysis of high-speed trains moving on bridges with foundation settlements. *Ingenieur. Archiv.* **2012**, *83*, 281–291. [[CrossRef](#)]
15. Feng, Y.-L.; Jiang, L.-Z.; Zhou, W.-B.; Lai, Z.-P.; Chai, X.-L. An analytical solution to the mapping relationship between bridge structures vertical deformation and rail deformation of high-speed railway. *Steel Compos. Struct.* **2019**, *33*, 209–224. [[CrossRef](#)]
16. Gou, H.-Y.; Ran, Z.-W.; Yang, L.-C.; Bao, Y.; Pu, Q.-H. Mapping Vertical Bridge Deformations to Track Geometry for High-speed Railway. *Steel Compos. Struct.* **2019**, *32*, 467–478. [[CrossRef](#)]
17. Al Shaer, A.; Duhamel, D.; Sab, K.; Foret, G.; Schmitt, L. Experimental settlement and dynamic behavior of a portion of ballasted railway track under high speed trains. *J. Sound Vib.* **2008**, *316*, 211–233. [[CrossRef](#)]
18. Lai, Z.; Jiang, L.; Liu, X.; Zhang, Y.; Zhou, W. Analytical investigation on the geometry of longitudinal continuous track in high-speed rail corresponding to lateral bridge deformation. *Constr. Build. Mater.* **2020**, *268*, 121064. [[CrossRef](#)]
19. Ahmari, S.; Yang, M.; Zhong, H. Dynamic interaction between vehicle and bridge deck subjected to support settlement. *Eng. Struct.* **2015**, *84*, 172–183. [[CrossRef](#)]
20. Chen, Z.; Zhai, W.; Cai, C.; Sun, Y. Safety threshold of high-speed railway pier settlement based on train-track-bridge dynamic interaction. *Sci. China Technol. Sci.* **2014**, *58*, 202–210. [[CrossRef](#)]
21. Lamas-Lopez, F.; Cui, Y.-J.; Calon, N.; D’Aguiar, S.C.; Zhang, T. Impact of train speed on the mechanical behaviours of track-bed materials. *J. Rock Mech. Geotech. Eng.* **2017**, *9*, 818–829. [[CrossRef](#)]
22. Ngamkhanong, C.; Ming, Q.Y.; Li, T.; Kaewunruen, S. Dynamic train-track interactions over railway track stiffness transition zones using baseplate fastening systems. *Eng. Fail. Anal.* **2020**, *118*, 104866. [[CrossRef](#)]
23. Zhai, W.; Han, Z.; Chen, Z.; Ling, L.; Zhu, S. Train-track-bridge dynamic interaction: A state-of-the-art review. *Veh. Syst. Dyn.* **2019**, *57*, 984–1027. [[CrossRef](#)]
24. Wang, D.; Luo, J.; Li, F.; Wang, L.; Su, J. Research on dynamic response and fatigue life of tunnel bottom structure under coupled action of train load and groundwater. *Soil Dyn. Earthq. Eng.* **2022**, *161*, 107405. [[CrossRef](#)]
25. Xiang, P.; Huang, W.; Jiang, L.; Lu, D.; Liu, X.; Zhang, Q. Investigations on the influence of prestressed concrete creep on train-track-bridge system. *Constr. Build. Mater.* **2021**, *293*, 123504. [[CrossRef](#)]
26. Jiang, L.-Z.; Liu, L.-L.; Zhou, W.-B.; Liu, X.; Liu, C.; Xiang, P. Mapped relationships between pier settlement and rail deformation of bridges with CRTS III SBT. *Steel Compos. Struct.* **2020**, *36*, 481–492. [[CrossRef](#)]
27. Feng, Y.; Hou, Y.; Jiang, L.; Zhou, W.; Li, H.; Yu, J. Failure mode of interlayer connection of longitudinally-connected ballastless track-bridge system under uneven pier settlement. *Constr. Build. Mater.* **2022**, *351*, 128805. [[CrossRef](#)]
28. Ye, X.; Yan, J.; Wang, Y.; Lu, L.; He, R. A Novel Capsule Convolutional Neural Network with Attention Mechanism for High-Voltage Circuit Breaker Fault Diagnosis. *Electr. Power Syst. Res.* **2022**, *209*, 108003. [[CrossRef](#)]
29. Luo, X.; Chen, M. A Novel SiC MOSFET Module for High-power Soft-switching Converter. In Proceedings of the 2021 IEEE Energy Conversion Congress and Exposition (ECCE), Virtual, 10–14 October 2021; pp. 5263–5268. [[CrossRef](#)]
30. Chen, Z.; Bi, L.; Zhao, J. Comparison of single-pier settlement model and multi-pier settlement model in solving train-track-bridge interaction. *Veh. Syst. Dyn.* **2020**, *59*, 1484–1508. [[CrossRef](#)]
31. Zhou, L.; Li, X.; Chen, W.; Shi, T. A Modified Method for Initial Rotor Position Detection of Brushless DC Motor Based on Voltage Vector Injection. In Proceedings of the 2021 IEEE 4th Student Conference on Electric Machines and Systems (SCEMS), Hangzhou, China, 1–3 December 2021; pp. 1–6. [[CrossRef](#)]
32. Borchers, J.S.; Campbell, C.R.; Van Scoy, S.B.; Clark, M.J.; Anand, R.K. Front Cover: Redox Cycling at an Array of Interdigitated Bipolar Electrodes for Enhanced Sensitivity in Biosensing (ChemElectroChem 18/2021). *ChemElectroChem* **2021**, *8*, 3427. [[CrossRef](#)]
33. Yue, X.; Yang, J.; Gao, J.; Xu, X.; Jing, Y.; Wang, X.; Li, W.; Li, X. Wearable hydroxylated MWCNTs/ecoflex composite strain sensor with high comprehensive performance based on electron irradiation. *Compos. Sci. Technol.* **2022**, *226*, 109537. [[CrossRef](#)]
34. Chen, X.; Wang, X.; Chen, Y.; Wang, H. A Novel SAR Image Target Recognition Algorithm under Big Data Analysis. *Wirel. Commun. Mob. Comput.* **2021**, *2021*, 4556157. [[CrossRef](#)]